Journal of Bio- and Tribo-Corrosion (2020) 6:128
https://doi.org/10.1007/s40735-020-00422-2

Evaluation of the corrosion inhibitory effect of Napoleonaea Imperalis leaf extract on mild steel in a 1.3 M H_2SO_4 medium

L. N. Emembolu[1] · O. D. Onukwuli[1] · C. J. Umembamalu[1] · C. O. Aniagor[1]

Received: 21 February 2020 / Revised: 27 August 2020 / Accepted: 11 September 2020 / Published online: 23 September 2020

Abstract

The study investigated the corrosion inhibitory effect of *Napoleonaea imperalis* leaf extracts (*'NI'*) on Mild steel (M-steel) in 1.3 M H_2SO_4. Weight loss, potentiodynamic and electrochemical impedance spectroscopy (EIS) at 303 K–343 K were the investigative approaches adopted in the study. The resultant oxide from the study was characterized using Fourier transform infrared spectroscopy (FTIR) and Scanning electron microscope (SEM). Meanwhile, the experimental results were validated using theoretical calculations. The experimental findings showed that by increasing the inhibitor concentration (from 0.2 to 1.0 g/L) at a low operational temperature of 303 K, an increased inhibition efficiency (from 47.93 to 85.54%) was observed. The organic functional groups responsible for inhibition effect were identified in the FTIR result. Similarly, the SEM result showed the occurrence of significant transformation on the M-steel surface due to effective corrosion inhibition by *'NI'*. The range of values of the free energy of adsorption, ΔG_{ads} (− 12.88 to − 5.83 kJ/kmol) and heat of adsorption, Q_{ads}, (− 24.10 to − 5.10 KJ/kmol) indicates the occurrence of physisorption process. The negative values obtained for the free energy of adsorption is an indication for a spontaneous and exothermic inhibition process. Tafel polarization curves depicted the inhibitor used in the study as a mixed-type. Similarly, the density functional theory (using molecular dynamic simulations) suggested a dependent adsorption process with coordinate bonds via metal/inhibitor interface. The study succinctly demonstrated an excellent inhibition performance of *'NI'* in M-steel corrosion.

Keywords Acid solution · Corrosion inhibition · *Napoleonaea imperalis* · Quantum chemical study · Weight loss

Abbreviations

'NI'	*Napoleonaea imperalis leaf extract*
ΔG_{ads}	Free energy of adsorption
Δw	Weight loss
a	Attractive parameter
C	Inhibitor concentration
C_{dl}	Non-ideal double-layer capacitance
CR	Corrosion rate
E_a	Activation energy
E_{corr}	Corrosion potential
EIS	Electrochemical impedance spectroscopy
EIS	Electrochemical impedance spectroscopy
FTIR	Fourier transform infrared spectroscopy
i_{corr}	Corrosion current density
IE	Inhibition efficiency
K_{ads}	**A**dsorption equilibrium
M-steel	Mild steel
n	Phase shift coefficient
Q_{ads}	Heat of adsorption
R_{ct}	Charge transfer resistance
RN	Reaction number
R_s	Solution resistance
SEM	Scanning electron microscope
T_i	Initial experimental temperature (k)
T_m	Maximum experimental temperature (K)
x	Size parameter
DFT	Density functional theory
MMO	Morpholine, 4-methyl-4-oxide
E_{HOMO}	Energy of the highest occupied molecular orbital
E_{LUMO}	Energy of the lowest occupied molecular orbital
ΔE	Energy gap
HOMO	Highest occupied molecular orbital
LUMO	Lowest occupied molecular orbital
E_{ads}	Adsorption energy

✉ L. N. Emembolu
ln.emembolu@unizik.edu.ng

✉ C. O. Aniagor
co.aniagor@unizik.edu.ng

[1] Department of Chemical Engineering, Nnamdi Azikiwe University, Awka, Nigeria

List of symbols

α	Lateral interaction term explaining the nature of adsorbed layer
Θ	Surface coverage

1 Introduction

M-steels are carbon steel which is used mostly as material for piping constructions in chemical and petrochemical industries [1]. After certain usage period, the thickness of the surface of these pipes slowly decreases (via corrosion) owing to the deterioration caused by the acid descaling, pickling, oil well acidifying, industrial acid cleaning, et.c [2, 3]. The corrosion of these alloys could cause great economic wastage [4] and may in some cases result in untold structural failure [5]. Such structural failures and emergencies may result in uncontrollable loss of human life and other social-economic losses [5].

Corrosion inhibitors are one of the most effectual alternatives to protect M-steel against corrosion, especially in acidic media, due to its advantages of low-cost, high effectiveness and wide applicability [6]. Corrosion mitigation in metallic components ultimately extends their usage efficiency and lifetime [7]. It could also give rise to several socio-economic benefits, as well as reduce the incidences of ecotoxicity associated with metal dissolution and corrosion [8]. Therefore, ensuring corrosion inhibition in metals utilized in industrial operations is plausible and should be given attention. The influence of relevant functional groups of the inhibitor on its corrosion inhibition performance has been reported. Also, the physicochemical constituents of the molecule, steric effects, electronic density of atoms and the interaction between surface atoms have been reported as key factors in corrosion inhibition process [9, 10]. Natural organic compounds comprising of heteroatoms with high electron density like oxygen, phosphorus, nitrogen, sulphur, and/or those having multiple bonds were considered in adsorption centres for effective inhibition [11–14]. The compounds comprising sulphur and nitrogen in their molecular structure have shown better inhibition when compared with those lacking either of these atoms [15–17]. The most active corrosion inhibitors contain some of the potential functional groups like hydroxyl (–OH) and nitro ($–NO_2$), pie electron and heterocyclic compounds [15–17]. The environmental toxicity of the readily available and commonly used synthetic corrosion inhibitors have fueled the search for eco-friendly corrosion inhibitors.

Application of various inhibitors for providing the most effective metal corrosion inhibition has been widely acknowledged. The inhibiting impact of extracts from curcumin, parsley and cassia bark extract carbon steel corrosion in 0.5 M H_2SO_4 solution has been investigated [18]. The result showed that the percentage inhibition efficiency increases with increase in the concentration of the extract, probably due to its horizontal adsorption on the C-steel surface. Apart from plant extracts, the inhibition effect of expired drugs and ionic liquids have also been studied. Efficient inhibition of mild steel corrosion in 1.0 M sulfuric acid medium using expired antibiotics (Ampicillin and Flucloxacillin) was reported [19]. The high inhibition efficiencies recorded in the study was due to the efficient adsorption of the drug species onto the surface of the mild steel; thus, resulting in the formation of protective layers. Similarly, Abdallah, et al. [20] studied the inhibition effect of expired Acyclovir and Omeprazole as inhibitors for the dissolution of Sabic iron in 1.0 M HCl. The experimental finding showed that the drugs were efficient for moving the pitting potential of the Sabic iron to a more noble value. The application of Schiff bases as inhibitors in aluminium corrosion in 1 M H_2SO_4 medium via mass loss and electrochemical techniques were reported as effective [21]. El Ouadi et al. [22] also studied the inhibiting effect of palm oil from *Phoenix dactylifera* seed on mild steel corrosion in hydrochloric acid medium. Furthermore, Al-Moubaraki, et al. [23] studied the corrosion behaviour and mechanism of mild steel/H_2SO_4 systems using hydrogen gas evolution. The study demonstrated that the corrosion mechanism is strongly related to the role of the SO_4^{2-} anion in the corrosion system.

Napoleonaea imperialis is a small, evergreen tropical tree in the lecythidaceae family and is native to West Africa. The plant is none food competing and its leaf extract contains some phytochemicals like saponins, alkaloids, glycosides and proteins [24]. These phytochemicals have structures similar to those of conventional corrosion inhibitors, hence their potential to inhibit metals/alloys corrosion. As opposed to chemical-based inhibitors, *'NI'* is a readily available, ecologically acceptable, and a renewable inhibitor. Using thermometric measurement, Chahul, et al. [25], investigated the efficacy of *Napoleonaea imperialis* leaf extract for inhibiting aluminium dissolution in 0.5 and 1.0 M HCl media. Similarly, Chahul, et al. [26] studied the effect of *Napoleonaea imperialis* seed extract on the corrosion of mild steel in 1.0 M solution of HCl using weight loss measurements.

This study, therefore, sets to investigate the corrosion inhibitory effect of eco-friendly *'NI'* on mild steel corrosion in H_2SO_4 medium. To our best knowledge and judging from our literature review, there is no reported work on the use of *'NI'* as a corrosion inhibitor for mild steel in H_2SO_4 medium. Furthermore, to ensure a holistic investigation, the study adopted weight loss, electrochemical and quantum chemical measurement techniques. These measurement approaches are not commonly reported simultaneously in a single research article; thus, justifying the essence of the work. Also, regarding social relevance, the study aims at communicating demonstrable and informed evidence about the effectiveness of *'NI'* for inhibiting the corrosion of

mild steel (in a relatively aggressive acidic medium, 1.3 M H_2SO_4) to the academic research community and the general public. The experimental data reported in the study will also be useful for assessing the potential application of *'NI'* as corrosion inhibition at an industrial scale.

2 Material and Methods

2.1 Preparation of the Plant Extract

Napoleonaea imperialis leaves were collected from Onitsha in Anambra State of Nigeria. The leaves were dried for 3 days and ground into powder. In the process of extraction, 40 g of *Napoleonaea imperialis* leaves were weighed and soaked in 500 mL of ethanol for 48 h before separation. The constituents of the stock solution such as flavonoids, tannins, alkaloids, saponins, phenolics and steroids were determined using phytochemical analysis. All the reagents used in the study were high grade.

2.2 Metal Preparation

The mild steel used in this study has the following compositions of P (0.02%), Mn (0.11%), Si (0.02%), S (0.02%), Cu (0.01%), C (0.23%), Ni (0.02), Cr (0.01%) and Fe (99.56%). The mild steel which has the following dimensions (5 cm × 4 cm × 0.18 cm) was mechanically cut into coupons. The coupons were cleaned followed by polishing with emery paper of different sizes to expose the shiny polished surface. To remove any oil and organic impurities, the coupons were degreased with acetone and finally washed with distilled water, dried in air and then stored in a desiccator before use.

2.3 Instrumental Analysis

2.3.1 Fourier Transform Infrared Spectrophotometer (FTIR)

FTIR analysis was done on pure sample to identify the active functional group before the corrosion process. The mild steel coupons were introduced in the inhibited medium. After the corrosion study, the corrosion products were collected and subjected to Fourier transform infrared spectroscopy using KBr pellet method (SHIMADZU Model IR affinity-1) to identify the functional groups present in the corrosion products.

2.3.2 Scanning Electron Microscopy (SEM)

The surface morphology of the corroded coupons was analysed at Ahmadu Bello University, Zaria, using the scanning electron microscope (Manufactured by Phenom-world Eindhoven, Netherlands). The surfaces of the mild steel coupons immersed in inhibited and uninhibited acid environments were examined.

2.4 Thermometric Approach

This experiment was done using thermostat at 373 K for the metal specimen. The temperature of the system was regularly monitored to ensure that a stabilized temperature value was reached. The reaction number (RN) was calculated using Eq. (1) as previously described [27, 28].

$$RN = \frac{T_{m-T_i}}{t} \tag{1}$$

where T_m and T_i denote the maximum and initial temperatures in K, t is the duration in minutes taken to reach T_m.

2.5 Gravimetric Method

The gravimetric technique was performed at temperatures of 303 K, 323 K and 343 K respectively. As described previously [10, 29], the weighed metal coupons were immersed in 250 mL beakers containing 200 mL of 1.3 M H_2SO_4 with inhibitor concentrations ranging from 0.2–1.0 g/L. The coupons were taken out hourly until 8 h and immersed in acetone, scrubbed with a bristle brush under running water, dried and re-weighed. The weight loss was calculated in grammes as the difference between the initial weight and the final weight after removal from free and inhibited test solutions respectively. The experimental readings were recorded. The weight loss (Δw), corrosion rate (CR) and inhibition efficiency (IE) and surface coverage, θ, were obtained using Eqs. (2–5), respectively [30].

$$\Delta w = w_i - w_f \tag{2}$$

$$\mathrm{CR} = \frac{w_i - w_f}{A_t} \tag{3}$$

$$\mathrm{IE}\ \% = \frac{\omega_0 - \omega_1}{\omega_0} \tag{4}$$

$$\theta = \frac{\omega_0 - \omega_1}{\omega_0} \tag{5}$$

where w_i and w_f are the initial and final weight of metal samples respectively; ω_1 and ω_0 are the weight loss values in presence and absence of inhibitor, respectively. A is the total area of the specimen and t is the immersion time.

2.6 Electrochemical Technique

The electrochemical experiment was conducted in a three-electrode corrosion cell using a VERSASTAT 300 complete DC voltammetry and corrosion system with V3 studio software for electrochemical impedance spectroscopy. Then, the potentiodynamic/galvanostat corrosion system with E-chem software was used for potentiodynamic polarization experiments. A graphite rod was used as a counter electrode and a saturated calomel electrode (SCE) was used as the reference electrode. The latter was connected via a luggins capillary. A mild steel specimen of $2cm^2$ dimension was used as working electrode. Impedance measurements were performed in aerated and unstirred solutions at the end of 1800s at 30 ± 1^0 C, over a frequency range of 100 kHz–0.1 Hz with a signal amplitude perturbation of 5 mV [27, 31]. The inhibition efficiencies (IE %) for different inhibitor concentrations were calculated from Nyquist plots using the Eq. (6).

$$\mathrm{IE}\% = \left(\frac{R_{\mathrm{ct(inh)}} - R_{\mathrm{ct}}}{R_{\mathrm{ct(inh)}}} \right) \times 100 \tag{6}$$

where R_{ct} and $R_{ct\ (inh)}$ denotes charge transfer resistance in the absence and presence of the inhibitor.

Polarization studies were carried out in the potential range ± 250 mV versus corrosion potential at a scan rate of 0.333 mVs^{-1}. Each test was run in triplicate to verify the reproducibility of the data. The inhibition efficiency was determined using Eq. (7).

$$IE\% = \frac{i_{corr(uninh)} - i_{corr(inh)}}{i_{corr(uninh)}} \times 100 \tag{7}$$

where $i_{corr\ (uninh)}$ and $i_{corr\ (inh)}$ are the corrosion current density values without and with inhibitors, respectively.

2.7 Quantum Chemical Calculations

All theoretical calculations were performed using the density functional theory (DFT) electronic structure programs Forcite and $DMol^3$ as contained in the Materials Studio 4.0 software (Accelrys, Inc.).

2.8 Evaluation of Heat of Adsorption and Activation Energy

The relationship between corrosion rates at different temperatures T_1 and T_2 as CR_1 and CR_2 can be used to calculate the activation energy as can be seen from the Arrhenius equation in Eq. (8). The heat of adsorption Q_{ads} (kJ mol^{-1}) was calculated using Eq. (9) [32].

$$\ln\left(\mathrm{CR}_1/\mathrm{CR}_2\right) = \left(E_a/2.303R\right)\left(1/T_1 - 1/T_2\right) \tag{8}$$

$$Q_{\mathrm{ads}} = 2.303R\left\{ \log\left(\frac{\theta_2}{1-\theta_2} \right) - \log\left(\frac{\theta_1}{1-\theta_1} \right) \right\} \times \frac{T_2 T_1}{T_2 - T_1} \tag{9}$$

where E_a is the activation energy, R denotes gas constant, θ_1 and θ_2 represent the degree of surface coverage at temperature T_1 and T_2. θ_1 and θ_2 was evaluated in Sect. 2.5 from Eq. (5).

2.9 Adsorption Isotherm Consideration

Adsorption isotherms provide information on the interaction among adsorbed molecules, as well as with the metal surface. The adsorption characteristics of *'NI'* on the mild steel surface was investigated using four (Flory–Huggins, Frumkin, Langmuir and Temkin) adsorption isotherm models, whose equations are presented in Eqs. 10–13, respectively. Assuming a direct relationship between inhibition efficiency and surface coverage, the values of thermodynamic properties were thus generated from the respective isotherm models.

$$\log\left(\frac{\theta}{C}\right) = \log K + x \log(1-\theta) \tag{10}$$

$$\log\left\{ C \times \left(\frac{\theta}{1-\theta} \right) \right\} = 2.303 \log K + 2 \propto \theta \tag{11}$$

$$\frac{K}{\theta} = \frac{1}{K_{\mathrm{ads}}} + C \tag{12}$$

$$\theta = \frac{2.303 \log K}{2a} - \frac{2.303 \log C}{2a} \tag{13}$$

where x is size parameter; C = inhibitor concentration; α = lateral interaction term explaining the nature of adsorbed layer; K_{ads} = adsorption equilibrium; 'a' = attractive parameter.

3 Results and Discussion

3.1 Infrared Spectroscopic Analysis

The observed peak for the FTIR examination of the *'NI'* (corrosion inhibitor) and corrosion product is presented in Table 1. It was seen that *'NI'* contained relevant functional groups (like C=O, O–H, and C–H stretching bands) required

Table 1 Noticeable peaks obtained from FTIR spectroscopy

'NI' leaves extract			Scratched mild steel oxide film		
Frequency (cm^{-1})	Intensity	Band assignment	Frequency (cm^{-1})	Intensity	Band assignment
1134.60	2.1934	C–O	983.68	3.7293	C–O
1258.44	2.3642	C–O	1168.84	3.3746	C–O
1567.08	1.9817	C–H	1415.72	2.5189	C–H
1938.60	2.7587	C=O	1724.32	2.0579	C=O
2367.24	1.7943	C–H	2156.36	2.4119	C–H
3601.80	1.735	O–H	3483.34	2.4463	O–H

Table 2 Effect of inhibitor concentration on IE (%) and RN

Inhibitor concentration g/L	RN/°Cmin^{-1}	IE %
0.0	0.0336	–
0.2	0.0180	47.93
0.4	0.0120	65.13
0.6	0.0058	80.01
0.8	0.0048	83.40
1.0	0.0040	85.54

for efficient inhibition. Furthermore, the evaluation of the corrosion product showed the presence of these inhibitor functional groups on its surface; thus, confirming an efficient corrosion inhibition by the *'NI'*. Also, some of the peaks shifted/decreased and some disappeared completely as can be seen from Table 1.

3.2 Scanning Electron Microscopy (SEM)

SEM images (Plate 1a, b) were obtained to investigate the observable changes in the surface morphology of mild steel in the absence and presence of *'NI'* inhibitor. Upon visual inspection and comparison, substantial morphological differences could be observed between Plate 1a, b. Plate 1a reveals that in the absence of *'NI'* inhibitor, the mild steel surface is highly damaged with pitted areas, typical of pitting corrosion. Meanwhile, in the presence of *'NI'* inhibitor, Plate 1b shows a relatively smooth surface in comparison to Plate 1a. Hence, the pits disappeared, leaving a smooth mild steel surface that is almost corrosion free even in the relatively concentrated acidic medium (1.3 M H_2SO_4). This observation could have resulted from the formation of an adsorbed protective film of *'NI'* leaf extracts on the mild steel surface; thus, inhibiting its corrosion.

3.3 Thermometric Result

Thermometric measurement provides an instantaneous corrosion measurement of a system [33]. Table 2 presents the variation between inhibition efficiency (IE), inhibitor concentration (*C*) and the reaction number (RN). It was observed that an increased inhibitor (*'NI'*) concentration caused a decrease in RN values, thus resulting in an improved inhibition efficiency. This suggests an inverse relationship between the inhibition efficiency and the reaction number. Meanwhile, the RN values is referred to as the relative measure of the degree of corrosion retardation [34]. This observation could be attributed to an increased number of the inhibitor molecules necessary for blocking the corrosion reaction sites. This form of reaction site blockage tends to lower the reaction number (RN) and consequently lower corrosion rate by reducing the surface area available for acid attack on the metal surface [29, 35]. Inhibition efficiency obtained in the study ranged from 47.93–85. 54%, hence, an increase in inhibitor concentration from 0.2 to 1.0 g/L caused about 38% (from 47.93 to 85.54%) improvement in the inhibitor efficiency (see Table 2). This illustrates an effective and efficient inhibition process by the *'NI'*. Therefore, the highest inhibition efficiency achieved in the study was 85.54% at 1.0 g/L.

3.4 Gravimetric Result

Equations 2–5 were used to calculate the corrosion rate, inhibition efficiency, surface coverage, and weight loss of mild steel in H_2SO_4 at 303–343 K and the obtained results were presented in Table 3. By visual inspection, Table 3 reveals that high *'NI'* concentrations resulted in increased adsorption site availability, thus making for faster and improved adsorption of the active constituents of the inhibitor on the surface of the corroding metal. These adsorbed active constituents ultimately improved the corrosion inhibition effect by forming an insoluble protective layer on the mild steel surface. The study also demonstrated that temperature increase negatively impacted the effectiveness of the corrosion inhibitor, as well as the entire inhibition process. The observed reduction of inhibition efficiency at high-temperature corrosion study is attributed to a decrease in surface coverage. The surface coverage decrease, however, results from the breaking of the heterocyclic bonds in the *'NI'* at high temperature; thus denaturing them [28, 36]. The maximum inhibition efficiency achieved in the study signifies the efficacy of *'NI'* as M-steel corrosion inhibitor in aqueous

Table 3 Obtained weight loss data for inhibited and non-inhibited process

Time/hr	Temp (K)	Inhibitor conc (g/L)	Weight loss (g)	CR (mg/cm^{2}hr)	θ	IE (%)
8	303	0.0	0.027	0.084	–	–
		0.2	0.017	0.053	0.4654	46.54
		0.4	0.013	0.041	0.6045	60.45
		0.6	0.007	0.022	0.7154	71.54
		0.8	0.007	0.022	0.7615	76.15
		1.0	0.007	0.022	0.8692	86.92
	323	0.0	0.043	0.134	–	–
		0.2	0.027	0.084	0.4275	42.75
		0.4	0.027	0.084	0.5725	57.25
		0.6	0.020	0.063	0.6884	68.84
		0.8	0.020	0.063	0.7101	71.01
		1.0	0.013	0.041	0.7246	72.46
	343	0.0	0.063	0.197		
		0.2	0.040	0.125	0.3776	37.76
		0.4	0.037	0.116	0.4755	47.55
		0.6	0.030	0.094	0.6503	65.03
		0.8	0.030	0.094	0.6524	65.24
		1.0	0.023	0.072	0.6643	66.43
4	303	0.0	0.020	0.125	–	–
		0.2	0.013	0.081	0.4454	44.54
		0.4	0.013	0.081	0.5792	57.92
		0.6	0.010	0.062	0.7154	71.54
		0.8	0.010	0.062	0.7462	74.62
		1.0	0.007	0.044	0.7485	74.85
	323	0.0	0.023	0.144	–	–
		0.2	0.017	0.106	0.4275	42.75
		0.4	0.013	0.081	0.5580	55.80
		0.6	0.013	0.081	0.6884	68.84
		0.8	0.010	0.062	0.6957	69.57
		1.0	0.010	0.062	0.7029	70.29
	343	0.0	0.033	0.206	–	–
		0.2	0.027	0.169	0.3456	34.56
		0.4	0.023	0.144	0.4755	47.55
		0.6	0.023	0.144	0.6385	63.85
		0.8	0.020	0.125	0.6434	64.34
		1.0	0.020	0.125	0.6455	64.55
1	303	0.0	0.040	0.083	–	–
		0.2	0.020	0.042	0.4354	43.54
		0.4	0.013	0.027	0.5846	58.46
		0.6	0.010	0.021	0.7154	71.54
		0.8	0.007	0.016	0.7462	74.62
		1.0	0.007	0.016	0.7538	75.38
	323	0.0	0.060	0.125	–	–
		0.2	0.033	0.069	0.4275	42.75
		0.4	0.027	0.056	0.5652	56.52
		0.6	0.023	0.048	0.6884	68.84
		0.8	0.017	0.035	0.7029	70.29
		1.0	0.013	0.027	0.7101	71.01
	343	0.0	0.090	0.188	–	–
		0.2	0.050	0.104	0.3133	31.33

Table 3 (continued)

Time/hr	Temp (K)	Inhibitor conc (g/L)	Weight loss (g)	CR (mg/cm^{2}hr)	θ	IE (%)
		0.4	0.047	0.098	0.4755	47.55
		0.6	0.040	0.083	0.6434	64.34
		0.8	0.033	0.069	0.6455	64.55
		1.0	0.030	0.063	0.6483	64.83

Table 4 Value of activation energy, E_a (kJ/mol) and heat of adsorption

Inhibitor conc. (g/L)	Activation energy (E_a) kJ/mol	Heat of adsorption (Q_{ads}) kJ/mol
0.0	62.0	–
0.2	67.7	– 5.0999
0.4	64.2	– 15.3450
0.6	69.2	– 22.3438
0.8	70.0	– 22.6029
1.0	80.4	– 24.0971

H_2SO_4 environment. Furthermore, the effect of increasing the *'NI'* concentrations on the weight loss of M-steel was also depicted in Table 3. As shown in Table 3, the increase in the *'NI'* concentration resulted in the corresponding decrease in M-steel weight loss. This observation implies that the *'NI'* presence significantly retarded the M-steel corrosion in 1.3 M H_2SO_4 media.

3.5 Heat of Adsorption and Activation Energy

The effect of temperature on the corrosion of mild steel in 1.3 M H_2SO_4 solution in the absence and presence of *'NI'* was investigated using weight loss measurements. The study was conducted at five different temperatures namely 303, 313, 323, 333 and 343 K, respectively and the results were recorded for 8 h. To avoid a clumsy presentation of results only the results obtained for 303–323 K were presented since no significant change in results were observed at temperatures beyond 323 K.

The variation of inhibition efficiency (I.E %) with temperature is presented in Table 3. From the results, it could be observed that I.E % decreases as the temperature increased. This observation is attributed to the desorption of the adsorbed *'NI'* active molecules (solubilization of the protective film) from the mild steel surface; thus, leading to a decrease in the I.E %. The effect of temperature on the corrosion rate was further estimated from the Arrhenius equation. The values of activation energy, E_a were calculated from the slope of the Arrhenius plots of log *C*r versus 1/*T* of mild steel in 1.3 M H_2SO_4 solution (plot not shown) and presented in Table 4.

The result from Table 4 revealed that E_a-values for the inhibited solution is greater than that of non-inhibited solution. The observed increase in the *E*a-values in the presence of *'NI'* confirms the formation of the higher energy barrier for corrosion process to happen, suggesting that adsorbed *'NI'* formed a passive film on the mild steel surface. This film prevented the charge/mass transfer reaction occurring on the metal surface which usually gives rise to corrosion [37, 38]. Also, the increased value of *E*a-values suggests that the mild steel corrosion rate was significantly repressed with the introduction of *'NI'*. This development was due to the formation of the insoluble metal-inhibitor complex at the mild steel surface [39]. The increase in the apparent activation energy for mild steel dissolution in inhibited solution may be inferred as physical adsorption [10].

The heat of adsorption (Q_{ads}) was equally evaluated from the variation of surface coverage with temperature [38, 40]. The negative values of heats of adsorption (Q_{ads}) show that the degree of surface coverage decreased with increase in temperature, which is as a result of physical adsorption mechanism [10, 38].

3.6 Adsorption Isotherm Behaviour

The characteristics of the adsorption of *'NI'* during the corrosion inhibition study was expounded using adsorption isotherms. An adsorption isotherm is thus an essential tool for understanding the mechanism of interaction between a given metal surface and the inhibitor [41]. The best fit isotherm model for describing the adsorption of *'NI'* onto mild steel in 1.3 M H_2SO_4 medium was obtained by fitting the corrosion rate, (CR) and the degree of surface coverage of the inhibitor, (θ) into the various adsorption isotherms models (Langmuir, Tempkin, Frumkin, and Flory Huggins adsorption isotherm) expressed in linear form as Eqs. 10–13.

Figure 1a–d show the plot of the various adsorption isotherm models considered in this study, while the R^2-values and other isotherm parameters obtained for each isotherm model as presented in Table 5, were used to determine the most suitable model. Flory–Huggins isotherm with R^2-values of 0.9996, gave the best isothermic description for the adsorption behaviour of *'NI'*, while, the Temkin isotherm with R^2-values of 0.9992 came in as the second-best fit model. Notably, the studies conducted at 303 K gave the

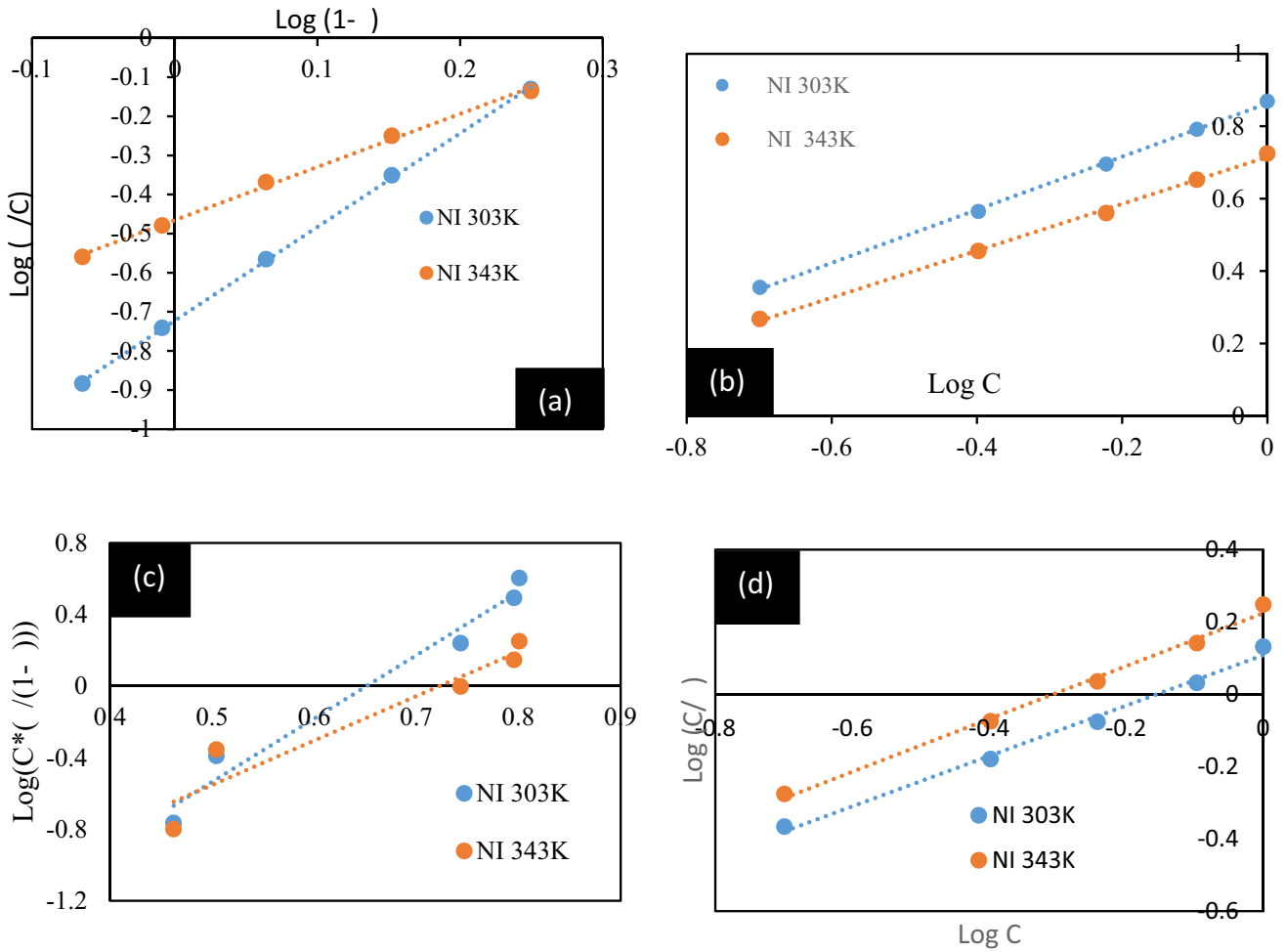

Fig. 1 Adsorption isotherm plots for **a** Flory–Huggins, **b** Temkin, **c** Frumkin and **d** Langmuir model

Table 5 Obtained isotherm parameters at varying temperatures

Flory–Huggins	Frumkin	Temkin	Langmuir
at 303 K			
$X = 2.491$	$\alpha = 1.976$	$a = 1.558$	$R^2 = 0.9936$
$R^2 = 0.9996$	$R^2 = 0.9719$	$R^2 = 0.9992$	$K_{ads} = 1.2391$
$K_{ads} = 0.1827$	$K_{ads} = 0.0749$	$K_{ads} = 0.0672$	$\Delta G^{\circ}_{ads} = -10.6598$
$\Delta G_{ads} = -5.8365$	$\Delta G_{ads} = -3.5905$	$\Delta G_{ads} = -3.3165$	Log $K = 0.0931$
Log $K = -0.7383$	Log $K = -1.1254$	Log $K = -1.1726$	
at 343 k			
$X = 1.357$	$\alpha = 1.916$	$a = 1.760$	$R^2 = 0.9924$
$R^2 = 0.9975$	$R^2 = 0.9596$	$R^2 = 0.9981$	$K_{ads} = 1.6478$
$K_{ads} = 0.3431$	$K_{ads} = 0.1015$	$K_{ads} = 0.0766$	$\Delta G_{ads} = -12.8801$
$\Delta G_{ads} = -8.4044$	$\Delta G_{ads} = -4.9305$	$\Delta G_{ads} = -4.1277$	Log $K = 0.2169$
Log $K = -0.4646$	Log $K = -0.9937$	Log $K = -1.1160$	

highest R^2-values when compared to those conducted at a higher temperature (343 K). This finding is unconnected with the possible denaturing of *'NI'* during high-temperature corrosion studies, as was already reported in Sect. 4.4

Considering the theory behind the best fit model, the Flory–Huggins isotherm parameter '*x*' (the size parameter) is a measure of the number of adsorbed water molecules substituted by a given inhibitor molecule [42]. However, the

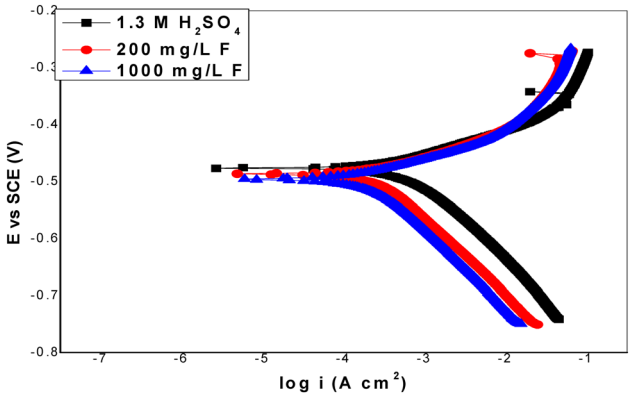

Fig. 2 A plot of potentiodynamic polarization in the presence and absence of different *'NI'* concentrations

Table 6 Electrochemical parameters derived from polarization curves

System	E_{corr} (mV vs SCE)	I_{corr} (μA/cm^2)	IE%
1.3 M H_2SO_4	− 509.7	168.5	–
200 mg/L NI	− 502.4	34.1	79.8
1000 mg/L NI	− 544.6	23.2	86.2

parameter 'x' obtained in the study has a positive value; thus showing that the bulk of the *'NI'* was on the metal surface [28]. The positive value obtained for the lateral interaction term ('α') of the Frumkin isotherm describes the molecular interaction in the adsorbed layer as a mutual inhibitor-metal surface attraction [40, 43]. Furthermore, the value of 'α' at 303 K is higher than the value at 343 K (Table 5), showing that the strength of the attractive behaviour of the *'NI'* extract reduces with temperature increase [40, 43]. The values obtained for molecular parameter 'a' were all negative indicating that repulsion forces occur between the metal surface and the adsorption layers [44]. The ΔG_{ads} values obtained were all negative, a proof of the spontaneous and exothermic nature of the reaction. The values of ΔG_{ads} ranged between − 3.3165 (KJ/mol) and − 12.8801(KJ/mol) demonstrating physisorption, since ΔG_{ads}-value less than − 20 kJ/mol show that the organic molecules of *'NI'* were adsorbed physically on the M-steel surface [45].

3.7 Potentiodynamic Polarization Results

The effects of *'NI'* on the mild steel inhibition in 1.3 M H_2SO_4 solution were investigated via potentiodynamic polarization techniques. The polarization plot was shown in Fig. 2. The values of corrosion current density (i_{corr}), corrosion potential (E_{corr}), and inhibition efficiency were obtained using Tafel extrapolation technique and are presented in Table 6. It was observed from Table 6 that the addition of *'NI'* to the acidic medium (1.3 M H_2SO_4 solution) resulted in a significant decrease in the i_{corr}-value and a slight shift in E_{corr} to a more negative value. Meanwhile, no substantial shift in the displacement was observed [44, 45]. Furthermore, a shift in the anodic and cathodic branches towards the region of lower current densities was observed. This shift could be due to the increase in inhibitor concentration; thus, reflecting the mixed-type nature of the *'NI'* inhibitor. It can also be deduced from the result that the adsorption of the inhibitor molecules onto the metal surface did not cause any alteration in the hydrogen evolution mechanism whereas the anodic dissolution of iron reaction mechanism was altered [45].

3.8 Electrochemical Impedance Spectroscopy Results

EIS measurements were studied to determine the electrochemical interactions of *'NI'* leaf extract molecules with the metal surface in H_2SO_4 aggressive solution. Figure 3a–c respectively provides the impedance spectra, the Bode modulus and Bode phase angle associated with the mild steel samples exposed to the inhibitor-free and inhibitor-loaded solutions. As shown in Fig. 3a, the radius of the impedance spectra semicircles was increased as the *'NI'* concentration increased. The adsorption of the active inhibitor components on the mild steel surface explains this observation [7, 46]**.** It is also clear that no much alteration was observed in the semicircles and the corrosion mechanism sequel to the introduction and subsequent solubilization of the *'NI'* powder in acidic media [47, 48]. The Nyquist diagram also portrays that the corrosion process is majorly a function of charge transfer since only one semicircle was observed in the respective acidic media of varying inhibitor concentrations [49, 50].

Nonetheless, variations in raw materials, surface impurity, electrode discontinuity and inhibitor adsorption, as well as electrode surface non-homogeneity could explain the observed deviations from a perfect semicircle [51, 52]. The experimental results were fitted into solution resistance (R_s), phase shift coefficient (n), charge transfer resistance (R_{ct}), non-ideal double-layer capacitance (C_{dl}) and inhibition efficiency to calculate the EIS parameters. The corresponding data obtained are presented in Table 7. Observations from this table highlighted slight increment in the Rs value after enhancement of the inhibitor concentration due to solution conductivity increment [53, 54].

Conversely, by augmenting the quantity of *'NI'* in the medium, the R_{ct} was substantially increased. This increment is indicative of organo-complex formation and inhibitor molecule adsorption on the steel substrate [55, 56]. In comparison, Table 7 explicitly indicates an improvement in "n" numerical values. As a result, the inhomogeneity of the mild

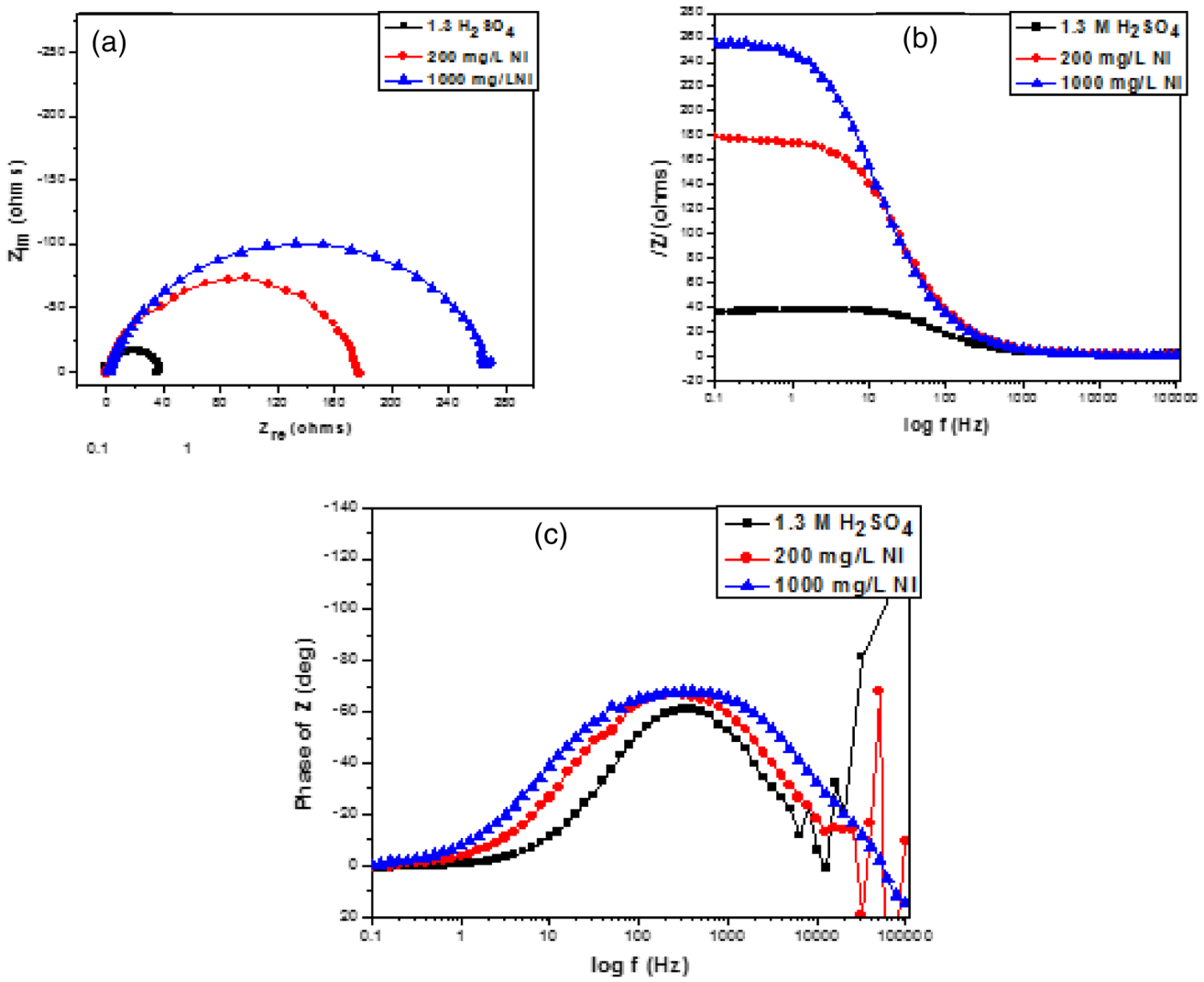

Fig. 3 Electrochemical impedance spectroscopy for mild steel in 1.3 M H_2SO_4 in the presence and absence of different concentration of NI extract: **a** Nyquist, **b** Bode modulus and **c** Bode phase angle

steel decreased and the metal surface became smoother after the development of a protective film on it [57, 58]. Evidence indicates that substantial reductions in C_{dl} levels (evaluated from Eq. 14) as the amount of inhibitor is increased suggest a reduction in local electrical constant and/or a rise in electrical dual-layer thickness [59].

Table 7 EIS parameters obtained from modelling of impedance data for mild steel specimen

System	*Rs* (Ωcm^2)	R_{ct} (Ω cm^2)	*N*	C_{dl} (μF cm^{-2})	IE%
1.3 M H_2SO_4	2.92	38.2	0.86	153.3	
200 mg/L NI	3.32	179.2	0.89	62.6	78.7
1000 mg/L NI	3.52	272.9	0.89	47.7	86

From Fig. 3b–c, it could be observed that there is only one time constant in Bode diagrams, proving that the inhibition of the mild steel corrosion is control by a charge transfer mechanism [8, 60]. The blank sample was found to have the lowest phase angle and impedance values, with the possibility of the occurrence of strong corrosion on the metal surface [61, 62]. After increasing the quantity of the *'NI'* extract in 1.3 M H_2SO_4 medium both parameters increased remarkably (Fig. 3c), illustrating inhibitive layer adsorption on the steel surface [63, 64]. The Helmholtz model, given by the Eq. 14.

$$C_{\mathrm{dl}} = \frac{\varepsilon \varepsilon_o A}{\delta} \tag{14}$$

where ε_o is the vacuum permittivity and ε the relative permittivity of the film.

3.9 Quantum Chemical Study: Interaction Between M-Steel Surface and Inhibitor

Quantum chemical calculation was utilized to determine the correlation between corrosion.

inhibition efficiency and molecular structure. Figure 4 shows the corrosion inhibiting performance of the active constituents, Morpholine, 4-methyl-4-oxide (MMO). To give further insight into the inhibitory mechanism of these active constituents on the mild steel surface, density functional theory (DFT) was employed. The approach is however useful for obtaining a precise, flexible and accurate calculation of the molecular geometries and electron distributions. Quantum chemical parameters such as E_{HOMO}, E_{LUMO}, the energy gap ΔE ($E_{LUMO} - E_{HOMO}$) and adsorption energy as obtained for *'NI'* active constituents were useful for predicting its (*'NI'*) activity toward the mild steel surface. These parameters were generated after geometric optimization for all nuclear coordinates. Frontier molecular orbital theory is very useful in predicting the adsorption centres for these molecules, as it is

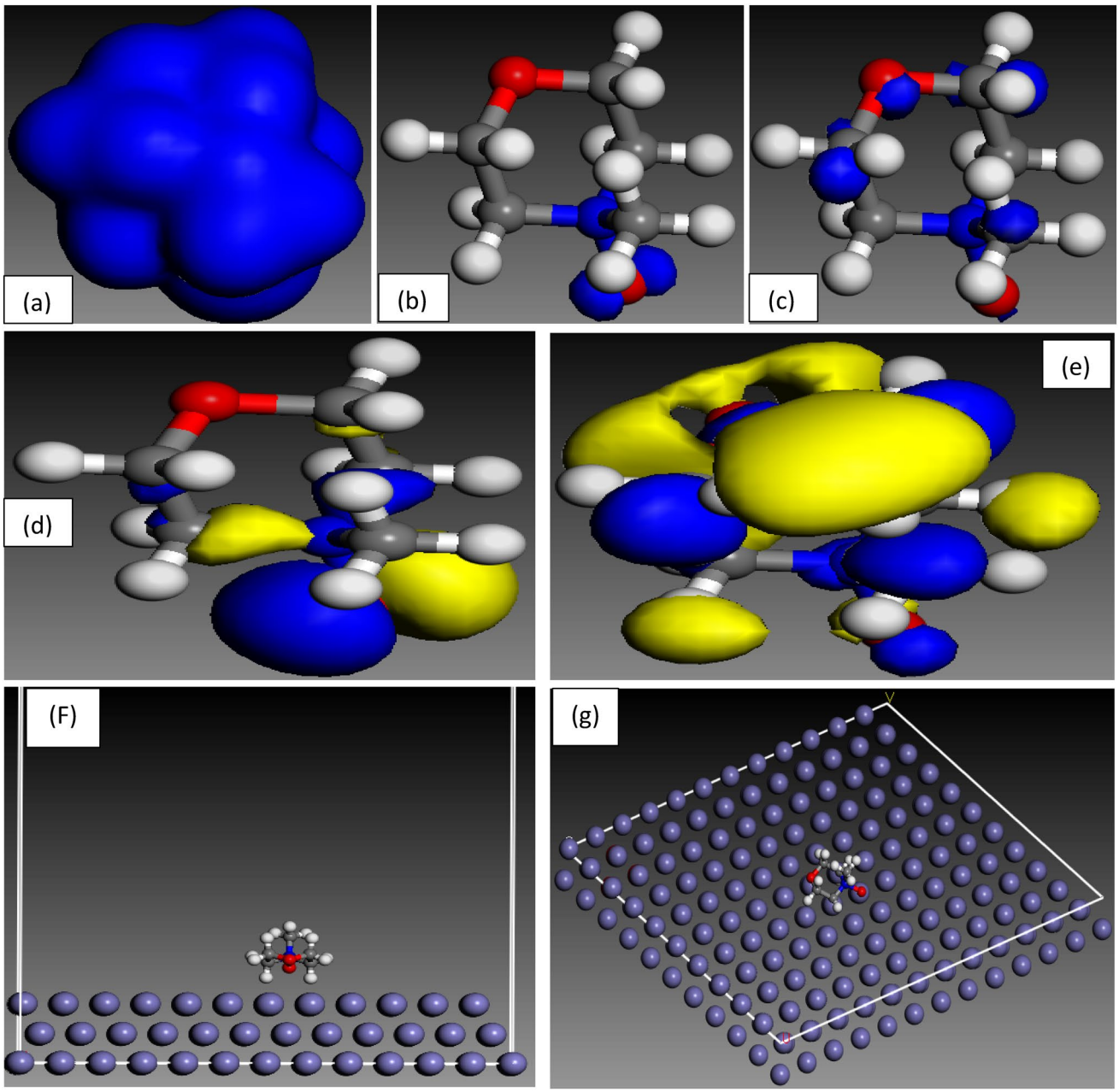

Fig. 4 Optimized molecular structures, HOMOs, and LUMOs **a** Electron density, **b** Electrophilic f (−), **c** Nucleophilic f (+), **d** HOMO, **e** LUMO **f** Side view of the Snapshot from molecular dynamics model. **g** Top view of the snapshot from molecular dynamics model

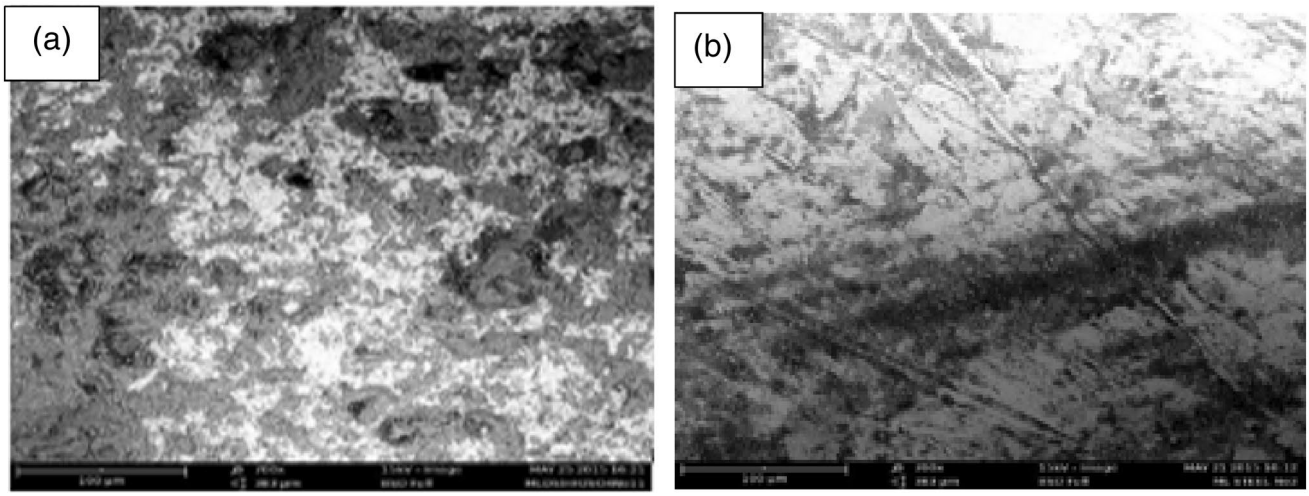

Plate 1 The micrograph of corroded mild steel surface in H_2SO_4 (**a**) in the absence of *'NI'* inhibitor, (**b**) in the presence of *'NI'* leaf extract

responsible for the interaction with the M-steel surface. Figure 4a–e**,** shows the total electron density, the Fukui functions for electrophilic (F^-), nucleophilic (F^+), the highest occupied molecular orbital (HOMO) and lowest unoccupied molecular orbital (LUMO), respectively. From Fig. 4d, e it was observed that the HOMO and LUMO energy orbitals were mostly occupied by the heteroatoms present in the molecules under study. The Mulliken charge analysis was used to estimate the adsorption centres of the inhibitors. Hence, it was observed that the adsorption of inhibitor molecules onto the M-steel surface is due to the donor–acceptor interaction between inhibitor molecules and the metal surface; since negatively charged atoms have a high adsorption tendency.

According to Emembolu, et al. [35], the electron-donating ability of an inhibitor molecule is associated with the E_{HOMO}. Therefore, high E_{HOMO}-values is indicative of the inhibitor molecules' tendency to donate electrons to the acceptor molecules with empty molecular orbitals. Conversely, the electron-acceptance ability of a molecule is related to the E_{LUMO} [35]. The lower value of E_{LUMO} indicates the easier acceptance of electrons from the metal surface and may lead to higher inhibition efficiency, though this has not been well established. The energy gap between the LUMO and HOMO energy levels, that is, ΔE of the molecule, is another important factor to determine the inhibition efficiency. The molecules with low ΔE values give better inhibition efficiencies because the excitation energy gap is more polarizable and is generally associated with chemical reactivity.

Table 8 provides some quantum chemical parameters (HOMO, LUMO, energy gap, molecular surface area and adsorption energy) related to the molecular electronic structures of the most stable conformations. The flat-lying adsorption orientation as shown in Fig. 4f, g, indicates the way the electron density is spread all around the molecule of the represented inhibitor. Forcite quench molecular dynamics was used to calculate different low energy adsorption configurations of MMA, the molecule on the metal surface [2, 65]. The metal crystal was cleaved along the (110) plane since it has a density packed surface and the most stabilization at this position. Calculations were carried out in a 12×10 supercell using the COMPASS force field and the Smart algorithm with NVE (microcanonical) ensemble, a time step of 1 fs, and simulation time 5 ps. The temperature was fixed at 350 K. Simulation was done using the optimized structure of the active constituent and the metal. The system was quenched every 250 steps. Figure 4f, g shows the optimized (lowest energy) adsorption structures for the active constituent in each case on the metal (110) surface from the simulation.

As proposed earlier, due to delocalization of the electron density, a flat-lying adsorption orientation was observed all around the chosen molecules. This orientation increases contact and this increases the degree of surface coverage. However, the properties calculated by quantum chemical approach gives information about the reactivity of these molecules but the reactivity cannot directly translate to

Table 8 Calculated quantum chemical properties for the most stable conformation of the active constituent of the inhibitor

Molecule	E_{HOMO} (eV)	E_{LUMO} (eV)	ΔE	Adsorption energy (Kcal/mol	Molecular surface area (Å)
Morpholine, 4-methyl-, 4-oxide	− 4.825	− 0.165	− 4.66	− 131.1	150.1

corrosion inhibition efficiency. This is because it involves more processes such as competitive adsorption, film formation, etc. Therefore, the generated correlations were not enough for optimizing the inhibitor structure [45, 58, 65]. The adsorption energy (E_{ads}) which is important in characterizing the adsorption of these molecules onto the Fe surface was estimated using Eq. 15.

$$E_{ads} = E_{total} - (E_{inhibitor} + E_{surface}) \quad (15)$$

where $E_{inhibitor}$, $E_{surface}$, and E_{total} represents the energy of a single molecule of these selected active components, the Fe slab without adsorption, and the total energy of the system containing a molecule and Fe surface, respectively.

3.10 *Napoleonaea Imperalis Corrosion Inhibition Mechanism in 1.3 M H_2SO_4 Medium*

The role of the SO_4^{2-} anions in describing the mechanism of mild steel corrosion in aqueous H_2SO_4 medium have been reported [23]. According to the study, mild steel corrosion is initiate when its protective surface film gets damaged by water molecules. Subsequently, the SO_4^{2-} anion causes dehydration, which is accompanied by electrostatic adsorption on the mild steel surface. As a result of the electrostatic interaction and attraction of double bonds to protons, a complex double layer of metal surface-anions-hydrogen ions may be developed; thus, facilitating hydrogen ions discharge. As a result of this loss of electrons via the discharge, the mild steel surface charge turns positive with enhanced anion adsorption; hence, dissolution/corrosion occurs.

Various mechanisms have been proposed for the inhibition of metallic corrosion in acid media [66]. However, a specified mechanism for the inhibition of mild steel corrosion is discussed herein. Upon the addition of *'NI'* inhibitor into the 1.3 M H_2SO_4 medium, the different chemical constituents of the '*NI'* extract would start to react with the dissolved ions originating from the mild steel surface. During this reaction, a stable organo-metallic complex would be formed, which will be subsequently adsorbed to the metal surface. The adsorption of this complex onto the M-steel surface is expressed as Eqs. 16–17.

$$(M-S) \rightarrow (M-S)^{2+} + 2e \quad (16)$$

$$(M-S)^{2+} +' NI' \leftrightarrow \left[(M-S) -' NI'\right]^{2+} \quad (17)$$

[*NB: 'M – S represents mild steel']

Generally, the stability of the adsorbed molecules/ions on the surface complex is the measure of the degree of corrosion inhibition recorded. Considering the high IE % of 85.54% recorded in the study, it could be concluded that the adsorption of the inherent phytochemical components of the *'NI'* extract led to the formation of a stable surface complex, which blocked the active sites on the surface of the mild steel, thereby reducing the corrosion rate. Furthermore, as already discussed in Sect. 4.3, the increase in the inhibitor concentration increased the amount of the surface complex formed; thereby resulting in improved corrosion inhibition.

3.11 Conclusions

The study demonstrated the efficacy of *Napoleonaea imperalis* leaf extracts ('*NI'*) as a corrosion inhibitor in 1.3 M H_2SO_4 medium. The inhibition efficiency increased with an increase in the *'NI'* concentration. *'NI'* was identified as a mixed-type inhibitor with major cathodic effectiveness, and it impeded the reduction of H^+ ions by simply hindering the reaction sites on the mild steel surface. For the anodic dissolution, the presence of *'NI'* resulted in the change of the anodic Tafel slopes. Meanwhile, it was observed that *'NI'* prevented mild steel corrosion through the spontaneous adsorption on the mild steel surface, and the process agrees with Flory–Huggins and Temkin isotherms. In theoretical view, the Morpholine, 4-methyl-4-oxide segment in *'NI'* molecule may act as the main site to donate electrons and form a coordinate bond with unoccupied d-orbitals of metal, while the dominant site accepts electrons from d-orbitals of metal to form a back-donating bond. This resulted in the observed lying-flat orientation of *'NI'* molecule to the mild steel surface. Furthermore, the smaller gap between E_{HOMO} and E_{LUMO} favours the adsorption of *'NI'* on mild steel surface and enhancement of corrosion inhibition. Molecular dynamics simulations revealed that PBI molecules flatly adsorb onto the iron surface, and the binding energy between PBI and iron surface is highest among the three studied inhibitor-iron systems.

Authors Contributions LNE wrote abstract, results and discussion, and conclusion. ODO edited and supervised the work. COA responded to the reviewer's queries and produced a revised version of the manuscript. CJU wrote the introduction and the experimental procedure.

Funding This research was supported by the authors.

Data Availability The data used in this research was generated at the Department of Chemical Engineering laboratory, Nnamdi Azikiwe University, Awka.

Compliance with Ethical Standards

Conflicts of interest The authors declare that they have no conflicts of interest.

References

1. Shetty P (2020) Schiff bases: An overview of their corrosion inhibition activity in acid media against mild steel. Chem Eng Commun 207(7):985–1029
2. Fu J et al (2012) Experimental and theoretical study on the inhibition performances of quinoxaline and its derivatives for the corrosion of mild steel in hydrochloric acid. Ind Eng Chem Res 51(18):6377–6386
3. Rodríguez-Valdez LM, Martínez-Villafañe A, Glossman-Mitnik D (2005) Computational simulation of the molecular structure and properties of heterocyclic organic compounds with possible corrosion inhibition properties. J Mol Struct (Thoechem) 713(1–3):65–70
4. Zhang F et al (2012) Performance and theoretical study on corrosion inhibition of 2-(4-pyridyl)-benzimidazole for mild steel in hydrochloric acid. Corros Sci 61:1–9
5. Subramanian C (2018) Localized pitting corrosion of API 5L grade A pipe used in industrial fire water piping applications. Eng Fail Anal 92:405–417
6. Umoren S et al (2008) Eco-friendly inhibitors from naturally occurring exudate gums for aluminium corrosion inhibition in acidic medium. Portugaliae Electrochimica Acta 26(3):267–282
7. Biswas A et al (2019) Biopolymer dextrin and poly (vinyl acetate) based graft copolymer as an efficient corrosion inhibitor for mild steel in hydrochloric acid: electrochemical, surface morphological and theoretical studies. J Mol Liq 275:867–878
8. Qassim RA, Mahdi SM, Majeed JG (2019) Using olive stone powder for steel corrosion inhibition. J Eng Sustain Deve 22(02 Part-1):1–9
9. Cruz J et al (2004) Experimental and theoretical study of 1-(2-ethylamino)-2-methylimidazoline as an inhibitor of carbon steel corrosion in acid media. J Electroanal Chem 566(1):111–121
10. Emembolu L, Onukwuli O (2019) Effect of Dialium guineense extracts on the corrosion inhibition of aluminum in alkaline solutions. J Mater Environ Sci 10(6):495–509
11. Gomez B et al (2006) Quantum chemical study of the inhibitive properties of 2-pyridyl-azoles. J Phys Chem B 110(18):8928–8934
12. Hussin MH, Kassim MJ (2011) The corrosion inhibition and adsorption behavior of Uncaria gambir extract on mild steel in 1 M HCl. Mater Chem Phys 125(3):461–468
13. Raja PB et al (2013) Neolamarckia cadamba alkaloids as eco-friendly corrosion inhibitors for mild steel in 1 M HCl media. Corros Sci 69:292–301
14. Zhang J et al (2011) Theoretical evaluation of corrosion inhibition performance of imidazoline compounds with different hydrophilic groups. Corros Sci 53(1):147–152
15. Ashassi-Sorkhabi H, Es'Haghi M (2009) Corrosion inhibition of mild steel in acidic media by [BMIm] Br Ionic liquid. Materi Chem Phys 114(1):267–271
16. Ebenso EE et al (2010) Quantum chemical studies of some rhodanine azosulpha drugs as corrosion inhibitors for mild steel in acidic medium. Int J Quantum Chem 110(5):1003–1018
17. Awad MK, Mustafa MR, Elnga MMA (2010) Computational simulation of the molecular structure of some triazoles as inhibitors for the corrosion of metal surface. J Mol Struct (Thoechem) 959(1–3):66–74
18. Abdallah M et al (2018) Some natural aqueous extracts of plants as green inhibitor for carbon steel corrosion in 0.5 M sulfuric acid. Green Chem Lett Rev 11(3):189–196
19. Alfakeer M, Abdallah M, Fawzy A (2020) Corrosion inhibition effect of expired ampicillin and flucloxacillin drugs for mild steel in aqueous acidic medium. Int J Electrochem Sci 15:3283–3297
20. Abdallah M, Fawzy A, Al Bahir A (2020) The effect of expired acyclovir and omeprazole drugs on the inhibition of sabic iron corrosion in HCl solution. Int. J. Electrochem. Sci 15:4739–4753
21. Nathiya R et al (2020) Synthesis, characterization and inhibition performance of schiff bases for aluminium corrosion in 1 MH 2 SO 4 solution. J Bio Tribo Corros 6(1):5
22. El Ouadi, Y., et al., *The Palm oil from seed of Phoenix dactylifera (Oil of both Deglet Nour and Kentichi) as a natural antioxidants and Environment-Friendly inhibitors on the Corrosion of mild Steel in HCl 1M*. Moroccan Journal of Chemistry, 2017. **5**(1): p. 5–1 (2017) 139–152.
23. Al-Moubaraki A, A Ganash, S Al-Malwi (2020) Investigation of the corrosion behavior of mild steel/H2SO4 systems. Morocc J Chem **8**(1): 8–1 (2020) 264–279.
24. Ibisi N, Okoroafor D, Amuta C (2017) Comparative study of mild steel corrosion inhibition of piper guineense leaves extract and vernonia amygdalina leaves extract in concentrated corrosive medium. IOSR J Appl Chem 10(5):70–78
25. Chahul HF, Ndukwe GI, Ogwu DO (2018) A thermometric study on the kinetics of the acid dissolution of aluminium in the presence of Napoleonaea imperialis seeds extract and iodide ions. Ovidius Univ Ann Chem 29(2):103–109
26. Chahul H, Ndukwe G, Ladan A (2019) Adsorption behaviour and corrosion inhibition effect of N. imperialis p. beauv (Lecythidaceae) seed extract on mild steel in 1.0 M HCl. ChemSearch J 10(1):25–32
27. Mejeha IM et al (2012) Experimental and theoretical assessment of the inhibiting action of Aspilia africana extract on corrosion aluminium alloy AA3003 in hydrochloric acid. J Mater Sci 47(6):2559–2572
28. Anadebe V et al (2018) Optimization and electrochemical study on the control of mild steel corrosion in hydrochloric acid solution with bitter kola leaf extract as inhibitor. S Afr J Chem 71(1):51–61
29. Emembolu LN, Onukwuli O (2019) Corrosion inhibitive efficacy of natural plant extracts on zinc in 0.5 M HCl solution. Pharma Chem J 6(2):62–70
30. Negm NA et al (2012) Gravimetric and electrochemical evaluation of environmentally friendly nonionic corrosion inhibitors for carbon steel in 1 M HCl. Corros Sci 65:94–103
31. Oguzie EE et al (2012) Natural products for materials protection: mechanism of corrosion inhibition of mild steel by acid extracts of Piper guineense. J Phys Chem C 116(25):13603–13615
32. Nwabanne J, Okafor V (2011) Inhibition of the corrosion of mild steel in acidic medium by Vernonia amygdalina: adsorption and thermodynamics study. J Emerg Trends Eng Appl Sci 2(4):619–625
33. Saka A, Ahmed O, Adekunle A (2020) On the use of factorial experiments for optimizing inhibition effect of acid extract of Gnetum Africana on copper corrosion. Int J Corros Scale Inhib 9(1):284–299
34. Umoren SA et al (2019) A critical review on the recent studies on plant biomaterials as corrosion inhibitors for industrial metals. J Ind Eng Chem 76:91–115
35. Emembolu L, Onukwuli O, Okafor V (2020) Characterization and optimization study of Epiphyllum oxypetalum extract as corrosion inhibitor for mild steel in 3 M H2SO4 solutions. World Sci News 145:256–273
36. Akalezi CO et al (2015) Rothmannia longiflora extract as corrosion inhibitor for mild steel in acidic media. Int J Indus Chem 6(4):273–284
37. Abd El-Lateef HM (2015) Experimental and computational investigation on the corrosion inhibition characteristics of mild steel by some novel synthesized imines in hydrochloric acid solutions. Corros Sci 92:104–117

38. Akalezi CO, Oguzie EE (2016) Evaluation of anticorrosion properties of Chrysophyllum albidum leaves extract for mild steel protection in acidic media. Int J Indus Chem 7(1):81–92
39. Fakrudeen S (2012) Electrochemical investigation of corrosion inhibition of AA6063 alloy in 1 M hydrochloric acid using Schiff base compounds. IOSR J Appl Chem 2(5):37–47
40. Eddy N (2010) Adsorption and inhibitive properties of ethanol extract of Garcinia kola and Cola nitida for the corrosion of mild steel in H2SO4. Pigment Resin Technol
41. Boumhara K et al (2019) Corrosion inhibition of mild steel in 0.5 MH 2 SO 4 solution by artemisia herba-alba oil. J Bio Tribo Corros 5(1):8
42. Rahal H, Abdel-Gaber A, Younes G (2016) Inhibition of steel corrosion in nitric acid by sulfur containing compounds. Chem Eng Commun 203(4):435–445
43. Sharma SK et al (2010) Corrosion inhibition and adsorption properties of Azadirachta indica mature leaves extract as green inhibitor for mild steel in HNO3. Green Chem Lett Rev 3(1):7–15
44. Ebenso E et al (2008) Inhibition of mild steel corrosion in sulphuric acid using alizarin yellow GG dye and synergistic iodide additive. Int J Electrochem Sci 3(12):1325–1339
45. Alibakhshi E et al (2018) Glycyrrhiza glabra leaves extract as a green corrosion inhibitor for mild steel in 1 M hydrochloric acid solution: experimental, molecular dynamics, Monte Carlo and quantum mechanics study. J Mol Liq 255:185–198
46. Zhang H, Chen Y (2019) Experimental and theoretical studies of benzaldehyde thiosemicarbazone derivatives as corrosion inhibitors for mild steel in acid media. J Mol Struct 1177:90–100
47. Asadikiya M, Y Zhong, M Ghorbani (2019) Corrosion Study of aluminum alloy 3303 in water-ethylene glycol mixture: effect of inhibitors and thermal shocking. Int J Corros
48. Hou B et al (2019) Effect of benzyl substitution at different sites on the inhibition performance of pyrimidine derivatives for mild steel in highly acidic solution. J Taiwan Inst Chem Eng 95:541–554
49. Ikeuba AI, PC Okafor (2019) Green corrosion protection for mild steel in acidic media: saponins and crude extracts of Gongronema latifolium. Pigment Resin Technol
50. Erna M, H Herdini, D Futra (2019) Corrosion inhibition mechanism of mild steel by amylose-acetate/carboxymethyl chitosan composites in acidic media. Int J Chem Eng
51. Ahmed SK, Ali WB, Khadom AA (2019) Synthesis and characterization of new triazole derivatives as corrosion inhibitors of carbon steel in acidic medium. J Bio Tribo Corros 5(1):15
52. Fadila B et al (2019) A study on the inhibition effect of expired amoxicillin on mild steel corrosion in 1N HCl. Mater Res Express 6(4):046419
53. Obot I et al (2019) Theoretical and experimental investigation of two alkyl carboxylates as corrosion inhibitors for steel in acidic medium. J Mol Liq 279:190–207
54. Guruprasad A et al (2019) Adsorption and inhibitive properties of seroquel drug for the corrosion of zinc in 0.1 M hydrochloric acid solution. Int J Indus Chem 10(1):17–30
55. El-Hajjaji F et al (2019) Effect of 1-(3-phenoxypropyl) pyridazin-1-ium bromide on steel corrosion inhibition in acidic medium. J Colloid Interface Sci 541:418–424
56. Jennane J et al (2019) Influence of sodium gluconate and cetyltrimethylammonium bromide on the corrosion behavior of duplex (α-β) brass in sulfuric acid solution. Mater Chem Phys 227:200–210
57. Abousalem AS, Ismail MA, Fouda AS (2019) A complementary experimental and in silico studies on the action of fluorophenyl-2, 2′-bichalcophenes as ecofriendly corrosion inhibitors and biocide agents. J Mol Liq 276:255–274
58. Dehghani A et al (2019) Electronic/atomic level fundamental theoretical evaluations combined with electrochemical/surface examinations of Tamarindus indiaca aqueous extract as a new green inhibitor for mild steel in acidic solution (HCl 1 M). J Taiwan Inst Chem Eng 102:349–377
59. Djouahra-Fahem D et al (2019) A comprehensive study on crude methanolic extract of Daphne gnidium L as effective corrosion inhibitors of mild steel induced by SRB consortium. J Bio Tribo Corros 5(1):18
60. Fouda AS et al (2019) Comprehensive investigations on the action of cationic terthiophene and bithiophene as corrosion inhibitors: experimental and theoretical studies. New J Chem 43(2):768–789
61. Dagdag O et al (2019) Anticorrosive properties of Hexa (3-methoxy propan-1, 2-diol) cyclotri-phosphazene compound for carbon steel in 3% NaCl medium: gravimetric, electrochemical, DFT and Monte Carlo simulation studies. Heliyon 5(3):e01340
62. Dhaundiyal P et al (2019) An investigation on mitigation of corrosion of mildsteel by Origanum vulgare in acidic medium. Bull Chem Soc Ethiop 33(1):159–168
63. Haldhar R, Prasad D, Bhardwaj N (2019) Extraction and experimental studies of Citrus aurantifolia as an economical and green corrosion inhibitor for mild steel in acidic media. J Adhes Sci Technol 33(11):1169–1183
64. Chen H et al (2019) Understanding the corrosion and tribological behaviors of CrSiN coatings with various Si contents in HCl solution. Tribol Int 131:530–540
65. Masoud M et al (2010) The role of structural chemistry in the inhibitive performance of some aminopyrimidines on the corrosion of steel. Corros Sci 52(7):2387–2396
66. Abdel-Gaber A et al (2006) Inhibitive action of some plant extracts on the corrosion of steel in acidic media. Corros Sci 48(9):2765–2779